HHS Public Access

Author manuscript

Biofabrication. Author manuscript; available in PMC 2020 November 04.

Published in final edited form as:

Biofabrication. ; 12(3): 035029. doi:10.1088/1758-5090/ab9492.

The Effect of BMP-mimetic Peptide Tethering Bioinks on the Differentiation of Dental Pulp Stem Cells (DPSCs) in 3D Bioprinted Dental Constructs

Ji Hoon Park[1], **Gregory J. Gillispie**[1], **Joshua S. Copus**[1], **Weibo Zhang**[2], **Anthony Atala**[1], **James J. Yoo**[1], **Pamela C. Yelick**[2,*], **Sang Jin Lee**[1,*]

[1]Wake Forest Institute for Regenerative Medicine, Wake Forest School of Medicine, Winston-Salem, NC 27157

[2]Department of Orthodontics, Tufts University, Boston MA 02111

Abstract

The goal of this study was to use 3D bioprinting technology to create a bioengineered dental construct containing human dental pulp stem cells (hDPSCs). To accomplish this, we first developed a novel bone morphogenetic protein (BMP) peptide-tethering bioink formulation and examined its rheological properties, its printability, and the structural stability of the bioprinted construct. Second, we evaluated the survival and differentiation of hDPSCs in the bioprinted dental construct by measuring cell viability, proliferation, and gene expression, as well as histological and immunofluorescent analyses. Our results showed that the peptide conjugation into the gelatin methacrylate (GelMA)-based bioink formulation was successfully performed. We determined that greater than 50% of the peptides remained in the bioprinted construct after 3 weeks *in vitro* cell culture. Human DPSC viability was >90% in the bioprinted constructs immediately after the printing process. Alizarin Red staining showed that the BMP peptide construct group exhibited the highest calcification as compared to the growth medium, osteogenic medium, and non-BMP peptide construct groups. In addition, immunofluorescent and quantitative reverse transcription-polymerase chain reaction (qRT-PCR) analyses showed robust expression of dentin sialophosphoprotein (DSPP) and osteocalcin (OCN) in the BMP peptide dental constructs. Together, these results strongly suggested that BMP peptide-tethering bioink could accelerate the differentiation of hDPSCs in 3D bioprinted dental constructs.

Keywords

3D bioprinting; bioink; dental pulp stem cells; tooth regeneration; tissue engineering

[*]CORRESPONDING AUTHORS: Pamela C. Yelick, Ph.D., Pamela.Yelick@tufts.edu, Tel: +1-627-636-240; Sang Jin Lee, Ph.D., sjlee@wakehealth.edu, Tel: +1-336-713-7288.

Competing financial interests: The authors declare that there are no competing financial interests.

1. Introduction

Craniofacial injuries and associated tooth loss is a significant health issue affecting millions of people in the US and worldwide (1, 2). Artificial dental implants are the current gold standard tooth replacement therapy; however, they lack many key properties of natural teeth and can be associated with complications leading to implant failure (3). Thus, a bioengineered tooth bud has been proposed as a superior alternative tooth replacement option (4-7). To facilitate the effort to create bioengineered teeth, great strides have been made in the fields of tissue engineering and regenerative medicine to create 3D bioprinting technologies capable of producing tissue constructs using a variety of cell types, biomaterials, and bioactive molecules (8-10). These technologies are able to deposit living cells into a desired shape or pattern to produce complex tissue architectures in a layer-by-layer fashion. Because the anatomical geometries seen in the human body are highly complex and not easily reproduced by other fabrication methods, 3D bioprinting strategies have significant potential to improve the efficiency of translating tissue engineering applications into the clinic.

Among many 3D printing methods, the microextrusion-based method is the most common for cell-based bioprinting approaches (9, 11). Hydrogels are a major component of bioinks used for cell-based bioprinting, due to the fact that they can be modified and formulated to provide optimized printability, structural integrity, and biological properties (12). Several hydrogels made of natural-derived materials, such as gelatin, collagen, alginate, and fibrin have been widely used for bioprinting applications (13-17). Gelatin methacrylate (GelMA) is a hydrogel modified from gelatin, which can be easily synthesized and cured by UV crosslinking. Due to this easy modification method, GelMA can be easily extruded by the bioprinter prior to crosslinking, as well as maintain its structural integrity via UV exposure after printing (18-22). Currently, a few approaches to developing tissue-specific bioinks to elicit desired cellular responses have been reported (23, 24). Typically, these approaches worked to provide significant control of tissue-specific cellular activities by creating 3D printed hydrogel constructs that closely matched the biomechanical properties of the targeted tissue and provided the proper cellular interactions (25-27). In addition, the tissue-specific microenvironment can be provided by these tissue-specific bioinks, where specific bioactive molecules such as growth factors, cytokines, ligands, and hormones are bound to the resulting scaffolds, and able to trigger biochemical responses for cellular activities (28-31).

Bone morphogenetic proteins (BMPs) are the most commonly used growth factors in the orthopedic field and have been approved by the Food and Drug Administration (FDA). BMP-2 has been shown to regenerate bone through osteogenic differentiation of osteoprogenitor cells and stem cells (32). Despite these advantages, a major drawback of BMP-2 is its relatively short half-life in the body, due to rapid degradation by proteinases. Therefore, repeated local delivery is required to achieve the biological activity necessary to reach therapeutic effects in clinical applications (33, 34). To avoid this issue, here we have used a synthetic BMP-2 mimetic peptide consisting of the amino acid sequence (KIPKASSVPTELSAISTLYL) (35), present in the native BMP-2, which is highly active during osteogenic differentiation. The advantages of this BMP-2 mimetic peptide include a

lower cost compared to the native BMP-2 and easy synthesis with the desired amino acid sequences that can be further customized as needed. Additionally, the short amino acid sequence of BMP-2 mimetic peptide makes it more stable and allows for efficient binding with hydrogels using a chemical reaction (36-38).

Our goal was to create a bioengineered dental construct by bioprinting human dental pulp stem cells (hDPSCs) and BMP-mimetic peptide tethering bioink. We hypothesized that the BMP-mimetic peptide tethering bioink could accelerate the differentiation of hDPSCs in the bioprinted dental constructs. In this study, we used a thiolated BMP-mimetic peptide that was directly conjugated into a GelMA-based bioink formulation. We examined the rheological properties, printability, and structural stability of the bioprinted dental constructs. To evaluate the biological properties and hDPSC differentiation in the bioprinted dental constructs, we measured cell viability and proliferation, and mineralized tissue matric production, and analyzed dental pulp stem cell differentiation marker expression by immunofluorescence and quantitative reverse transcription-polymerase chain reaction (qRT-PCR).

2. Materials and Methods

2.1. Materials

Type A gelatins derived from porcine skin tissue (~300g bloom and 90~110g bloom), sodium carbonate, sodium bicarbonate, methacrylate anhydride, hyaluronic acid (HA), photoinitiator (Irgacure 2959), and glycerol were purchased from Millipore Sigma (St. Louis, MO, USA). Bone morphogenetic protein (BMP)-mimetic peptide (KIPKASSVPTELSAISTLYL) with a -SH (cysteamide residue) at the C-terminal end, BMP mimic peptide conjugated fluorescein isothiocyanate (FITC-BMP), and FITC-BMP-SH was purchased from Genscript (Piscataway, NJ, USA). Live/Dead Cell Double Staining Kit, Alexa Fluor 594 and Alexa Fluor 488-conjugated secondary antibodies, Dako Antibody Diluent solution, and 0.45 μm syringe filters were purchased from Thermo Fisher (Waltham, MA, USA). Dentin sialophosphoprotein (DSPP, LFMb-21) and Osteocalcin (OCN, G-5) antibodies were purchased from Santa Cruz Biotechnology (Dallas, TX, USA). Vectashield Fluorescent mounting medium with DAPI was purchased from Vector Laboratories, Inc. (Burlingame, CA, USA). Trizol, sybrgreen, quantitative reverse transcriptase-polymerase chain reaction (qRT-PCR) kit, and primers were purchased from Eurofins Genomics (Louisville, KY). All cell culture related agents were purchased from HyClone (Logan, UT, USA) unless noted otherwise.

2.2. Synthesis of gelatin methacrylate (GelMA)

Gelatin methacrylate (GelMA) was synthesized by dissolving 10 g of type A gelatin (~300g Bloom) in CB buffer (0.25 M buffer comprising 7.95 mg/mL sodium carbonate and 0.73 mg/mL sodium bicarbonate in 1 L distilled water). The CB buffer was ensured to have a pH of 9.0 by adding either 1 M sodium hydroxide (NaOH) or hydrochloric acid (HCl) dropwise. Methacrylic anhydride (MAA) was then added in dropwise fashion (0.5 mL/min) to the gelatin solution using gentle magnetic stirring at 50°C, and the reaction was allowed to proceed for 3 h. Next, the GelMA solution (20 mL) was added to 80 mL of PBS (5×

dilution) to stop the reaction, and the solution was then dialyzed in distilled water using 12-14 kDa cutoff dialysis tubing (Spectra Por, Spectrum, NJ, USA) for 1 week at 37°C to remove salts and unreacted MAA, with daily water changes. Finally, the GelMA solution was lyophilized for 1 week and stored at −20°C until the use. Methacrylation (%) of the GelMA with different amounts of MAA was measured by ^{1}H NMR spectroscopy.

2.3. Conjugation of BMP-mimetic peptide into GelMA hydrogel

For measuring BMP-peptide conjugation, fluorescein isothiocyanate-labeled BMP-mimetic peptide (FITC-BMP) was used. FITC-BMP peptide and FITC-thiolated BMP peptide (FITC-BMP-SH) were mixed with 5 wt% GelMA hydrogel and 0.2 wt% photoinitiator (Irgacure 2959) in DI water, respectively. The BMP-GelMA solutions were placed in 1-cm diameter mold and crosslinked by UV exposure for 2 min. The FITC-labeled BMP-GelMA hydrogels were immersed in 2 mL of PBS in 24-well plates and shaken at 100 rpm and 37°C for up to 28 days. In each experiment, 1 mL of the solution was extracted from each well in the 24-well plates at determined time intervals and 1 mL of fresh PBS was immediately added into each well in the 24-well plates. The amount of FITC-BMP peptide was analyzed using a microplate reader (SpectraMax M5, 3860 N First Street, San Jose, USA) equipped with detection at 490 nm for FITC. Three independent experiments were performed on the GelMA hydrogel mixed with FITC-BMP peptide (nonconjugated BMP-GelMA) and FITC-BMP peptide-conjugated GelMA hydrogel. The amount of FITC released from the GelMA hydrogels was calculated and compared to a standard curve made with known concentrations of FITC.

2.4. Characterization of BMP-mimetic peptide-tethering GelMA hydrogels

GelMA and BMP-GelMA hydrogels were dissolved at 5 wt% with distilled water, respectively, and a photoinitiator (Irgacure 2959) was added to the hydrogels at 2 mg/mL and dissolved for 1 h under gentler shaking at 37°C. Before and after UV crosslinking, the rheological properties of the GelMA and BMP-GelMA hydrogels were compared using a rheometer (Discovery HR-2, TA Instruments, New Castle, DE, USA) with a temperature-controlled bottom plate and an 8-mm parallel plate measuring system. All measurements were conducted at 25°C with a gap distance of 0.3 mm at 1 Hz of oscillating frequency and 0.1% oscillating strain. The compressive mechanical properties of the GelMA and BMP-GelMA hydrogels were determined using a universal mechanical testing machine INSTRON 5544 (INSTRON 5544, INSTRON, Norwood, MA, USA) under uniaxial compression mode. The Instron was equipped with a 100 N load cell, and compression was conducted at 0.2 mm/min.

The swelling and degradation of the GelMA hydrogel and BMP-GelMA hydrogel constructs were also evaluated. A 0.5 mL volume of each hydrogel per well was placed in a 24-well plate and then UV crosslinked at 200 mV/cm^2 for 2 min. Samples were then transferred to individual wells of 12-well plates and submerged in 2 mL PBS for up to 28 days, with fresh PBS changed every 3 days. For the swelling test, samples were removed after 24 h, blotted dry, and weighed. These samples were then lyophilized for a minimum of 48 h and weighed again. The swelling ratio was calculated as the ratio of (wet weight)/(dry weight). For the degradation experiment, samples were collected at 0, 1, 3, 7, 14, 21, and 28 days and

weighed after a minimum of 48 h of lyophilization. All swelling and degradation experiments were conducted in triplicate.

2.5. Human dental pulp stem cell culture

Human dental pulp stem cells (hDPSCs) were obtained from Tufts University as previously published (4, 6, 7). Briefly, the dental pulp was harvested from human teeth extracted by clinicians at the Tufts University School of Dental Medicine for Orthodontic or other clinically relevant reasons. Dental pulps were minced into small pieces, enzymatically digested, filtered to single-cell suspensions, and plated in DMEM-F12 media. The cells were expanded into T175 flasks to passage 3 and cryopreserved until use. Prior to use, the hDPSCs were thawed, plated, passaged, and expanded in culture to P5 - P7. All primary cell lines were tested for odontogenic differentiation prior to being used for experiments.

Human DPSCs were cultured in normal growth medium (NGM) consisting of 440 mL DMEM/F12 medium supplemented by 50 mL FBS (HyClone, Logan, UT, USA), 25 μg/mL ascorbic acid (Millipore Sigma), 5 mL GlutaMAX™ Supplement (Life Technologies) and Antibiotic/antimycotic (A/A) (Life Technologies). The media was changed every 3 days. The cells were passaged after reaching approximately 80% confluence. Human DPSCs were expanded up to a maximum of passage 7 for all experiments. Alternatively, hDPSCs were cultured in osteogenic medium (OM) consisting of NGM plus osteogenic supplements (50 μg/mL ascorbic acid, 100 nM dexamethasone, and 10 mM β-glyceraldehyde-3-phosphate) to confirm their differentiation (Supplementary Figure 1).

2.6. GelMA and BMP-GelMA bioink preparation

The hDPSCs-laden bioink was prepared using 37.5 mg/ml gelatin, 30 mg/ml GelMA, 3.75 mg/ml HA, and 10% (v/v) glycerol. Briefly, HA and glycerol were dissolved in DMEM/high glucose without phenol red at 37°C with stirring overnight. Gelatin and GelMA were added to the HA/glycerol solution with a photoinitiator (Irgacure 2959) by gentle shaking at 37°C for 1 h. After the components were fully dissolved, the solution was sterilized by filtering through a 0.45 μm syringe filter. Lastly, the cells and 300 μg/mL BMP peptide were mixed with the bioink by gentle pipetting, using M1000E pipette (Gilson Microman, WI, USA) and capillary piston tips (Gilson Microman). The concentration of BMP peptide in the constructs was determined from literature (39-41).

2.7. Printing of hDPSCs-laden GelMA and BMP-GelMA constructs

The DPSC-laden dental constructs using both GelMA and BMP-GelMA bioinks were fabricated using our integrated tissue-organ printing (ITOP) system that contains an X, Y, Z-axis stage/controller, and multiple dispensing modules (8). A sterile plastic dispensing syringe was loaded with the cell-laden bioinks and cooled to 18°C in the cooling jacket dispenser. Both the GelMA and BMP-GelMA required approximately 130 to 160 kPa air pressure to extrude through a 330 μm inner diameter plastic nozzle. The bioprinting chamber was maintained at 22°C throughout the printing process. The dental constructs were printed in a layer-by-layer manner with a feed rate of 150 mm/min. After printing, the bioprinted dental constructs were crosslinked by UV exposure at 200 mV/cm^2 for 2 min. The solid cuboidal constructs had dimensions of 5 × 5 × 2 mm^3. The bioprinted dental constructs were

first cultured in growth media for 7 days to allow for the cells to proliferate and recover from the stress of the printing process. Next, the printed constructs were divided into three different groups - 1) NGM, 2) OM, and 3) OM without dexamethasone (OM-D) - to investigate the ability of the printed BMP-GelMA constructs to direct osteogenic differentiation of the embedded hDPSCs. OM was prepared with DMEM/F12 medium supplemented with 50 mL fetal bovine serum (FBS), 50 μg/mL ascorbic acid, 100 nM dexamethasone, 10 mM β-glyceraldehyde-3-phosphate, and 5 mL antibiotic/antimycotic (A/A). The constructs were then cultured for up to an additional 28 days, with media changes every two days.

2.8. *In vitro* cell viability and proliferation in the bioprinted dental constructs

To assess cell viability, the Live/Dead staining assay was performed on the dental constructs cultured *in vitro* for 1, 4, 7, and 14 days. First, the constructs were removed from culture media and washed 2-3 times at room temperature (RT) with PBS. Calcein AM and propidium iodide were then mixed in a 2:1 ratio in PBS to make the Live/Dead solution that was added to the constructs (1 mL each in a 24 well plate) and incubated at 37°C for 15 min. A Leica TCS LSI Macro Confocal microscope (Leica, Wetzlar, Germany) was used to detect fluorescence at 490 nm and 545 nm excitation for live and dead cells, respectively. The images were then merged and the ratio of Live to Dead cells was counted using ImageJ software (Ver. 1.51j). For the quantitative analysis of hDPSC proliferation, an AlamarBlue® assay was performed. The AlamarBlue® solution was added to cultured constructs containing cell culture media at a volumetric ratio of 1:9 and incubated at 37°C for 3 h. The solution was then removed, placed in individual wells of a 96 well-plate, and the absorbance was read on a microplate reader at 570 nm and 600 nm for reference.

2.9. Histological and immunofluorescent analyses

After 2 or 4 weeks of culture, the dental constructs were immediately fixed in 10% neutral buffered formalin for 24 h, embedded in paraffin, and sectioned into 7-μm thick sections. Mounted sections were deparaffinized by incubation in xylene 3 times for 5 min each, followed by rinsing in 100% ethanol for 2 min, and two additional rinses for 1 min, to remove any residual xylene. Sections were placed in 95% ethanol for 1 min for hydration, followed by rinsing in running tap water for 1 min. For hematoxylin and eosin (H&E) staining, slides were first stained in Gill's hematoxylin for 2 min to stain nuclei, and the excess stain was removed with running tap water for 2.5 min. Sections were then placed in Scott's tap water for bluing, the excess dye was removed by running tap water for 2 min, followed by immersion in 95% ethanol for another 2 min. Sections were then placed in the Working Eosin for 10 sec for cytoplasmic counterstain, the excess stain was removed by dipping in 95% ethanol 20 times, 15 sec per dip. An additional 60 dips in 100% ethanol were performed to dehydrate the sections, followed by alcohol clearing via 3 xylene rinses for 1 min each.

To measure the calcium production in the bioprinted dental constructs, Alizarin Red S staining was performed. Briefly, deparaffinized sections were hydrated to 50% ethanol, rinsed rapidly in deionized water, stained in Alizarin Red S solution for ~5 min, and removed when orange-red flakes formed indicating calcium phosphate deposition. Sections

were counterstained with light green for 1 min, dipped in 50:50 acetone:xylene solution for 10 sec, cleared in xylene, and mounted using resinous mounting medium. Calcified areas were quantified using ImageJ software (Ver. 1.51j) from three different samples.

For DSPP and OCN immunofluorescent staining, deparaffinized slides were dipped in sodium citrate buffer (10 mM sodium citrate, 0.05% Tween 20, pH 6.0) and heated at 110-120°C for 20 min to allow for antigen retrieval, followed by washing three times with PBS and blocking with Dako Antibody Diluent solution at room temperature for 1 h. The slides were subsequently incubated with mouse monoclonal IgG_{2b} DSPP or rabbit polyclonal IgG osteocalcin antibodies (1:50 dilutions) at 4°C overnight. Next, slides were rinsed three times with PBS and incubated with Alexa Fluor 594 or Alexa Fluor 488-conjugated secondary antibodies (1:100 dilution) for 1 h in a dark humidity chamber. Finally, cover slides were mounted with Vectashield Fluorescent mounting medium with DAPI reagent. The stained slides were viewed using a Leica DM 4000 B (Leica, Wetzlar, Germany) equipped with Olympus cellSens Dimension software (Olympus, 3500 Corporate Parkway, PA, USA). Antibody staining was quantified using ImageJ software (Ver. 1.51j) from three different samples.

2.10. RNA isolation and quantitative reverse transcription-polymerase chain reaction (qRT-PCR)

Total RNA was extracted and isolated from bioprinted samples by tissue homogenization followed by treatment with TRIzol RNA isolation reagent (Invitrogen, Carlsbad, CA, USA) according to the manufacturer's protocol. RNA concentrations and quality were monitored using a NanoDrop (Thermo Fisher Scientific, Waltham MA). Next, equal quantities of RNA from each sample were converted to cDNA using the QuantiTect Reverse Transcription Kit (Qiagen, Hilden, Düsseldorf, Germany) as per manufacturer’s protocol. cDNA samples were used for real-time PCR in triplicate using Power SYBR Green PCR Master Mix (Thermo Fisher Scientific, Waltham MA) according to the manufacturer’s suggested protocol. Bioprinted samples collected at time zero (one week after printing, but prior to switching to differentiation media) were used to determine baseline reads and GAPDH was used as the housekeeping gene. The relative fold change in mRNA expression was calculated using the delta-delta Ct ($2^{-\Delta\Delta Ct}$) method. Primer sequences are listed in Table 1.

2.11. Statistical analysis

Swelling, storage modulus, compressive stress, and Young's modulus values of GelMA and BMP-GelMA hydrogels were recorded in independent experiments for each data point. Cell viability was determined from Live/Dead images. Calcification area (H&E staining) and antibody-reactivity via immunofluorescence were obtained from independent experiments at 4 weeks. Results were analyzed with Origin Pro 8.5 (OriginLab Co, Northampton, MA), GraphPad Prism 8 (GraphPad Software, San Diego, CA), and SPSS software (SPSS, version 19; IBM, Armonk, NY). One-way or two-way analysis of variance (ANOVA), Tukey’s *post hoc* tests, and Student’s *t*-test were applied to mean comparisons. Variables are expressed as a mean ± standard deviation (SD), and differences between experimental groups were considered statistically significant at $P<0.05$. Data ($n=3$) presented was duplicated.

3. Results

3.1. Conjugation of BMP-mimetic peptide into GelMA hydrogel

The thiolated BMP-mimetic peptide was directly conjugated into GelMA hydrogel during the UV crosslinking process (Figure 1A,B). The methacrylation of the synthesized GelMA was measured by ^{1}H NMR spectroscopy (Figure 1C). The percent methacrylation of GelMA was dependent on the amount of MAA/gelatin (Figure 1D). In this study, 80% methacrylated GelMA was used. Additionally, FITC-labeled BMP peptide was used to confirm its conjugation to and stability in the GelMA hydrogel over time (Figure 2E). The GelMA hydrogel with nonconjugated BMP-peptide showed a rapid release of BMP-peptide from the GelMA hydrogel with more than 50% reduction in fluorescent intensity within 7 days. However, the BMP-conjugated GelMA hydrogel maintained greater than 40% fluorescent intensity after 28 days of incubation. This indicates that the BMP-peptide chemically bound to GelMA hydrogel was effectively conjugated and stabilized in the hydrogel.

3.2. Characterization of BMP-mimetic peptide-tethering GelMA hydrogels

The rheological properties of GelMA and BMP-GelMA hydrogels were analyzed, both before and after UV crosslinking, with a 1 Hz oscillating frequency and 0.1% oscillating strain (Figure 2A,B). GelMA and BMP-GelMA bioinks exhibited a ~2 kPa storage modulus (G') before UV crosslinking and exhibited a sharp increase to ~4 kPa after UV crosslinking. Both before and after crosslinking, the GelMA group had slightly higher storage modulus than the BMP-GelMA group. We expect that this is due to the conjugation of BMP-SH peptide to the double bonds in MA, which minimally, but not statistically significantly, reduces the number of double bonds available for crosslinking.

The Young's modulus measured after crosslinking showed that the BMP-GelMA group had a slightly lower Young's modulus than the GelMA without BMP, but the difference was not statistically significant (Figure 2C). BMP-peptide conjugation also did not impact the swelling ratio (Figure 2D) or mass loss (Figure 2E) of GelMA, with similar values obtained for both GelMA and BMP-GelMA constructs.

3.3. *In vitro* cell viability and proliferation in the bioprinted dental constructs

Based on our previous works, we optimized the printing parameters for the GelMA-based bioinks, and we were able to print the GelMA-based constructs containing hDPSCs with lattice and solid cuboidal structures (Figure 3A). The solid cuboidal constructs ($5 \times 5 \times 2$ mm^3) were used for further experiments. Cell viability was measured via Live/Dead staining of hDPSCs in bioprinted GelMA and BMP-GelMA constructs cultured for 1, 4, 7, and 14 days. In all of the groups, most of the hDPSCs were alive (green), with only a few dead cells detected (red) at each time point (Figure 3B). Analyses of 1-day constructs showed that live cells were evenly distributed after 3D cell printing in both groups. Over a period of 14 days, the cells began to exhibit a healthy, spread morphology. To quantify cell viability, the number of live cells were counted and expressed as a percentage of the total number of cells (Figure 3C). These results showed cell viability above 90% for all groups at all time points. Cell proliferation in the bioprinted dental constructs was also measured using AlamarBlue® assay (Figure 3D). In both GelMA and BMP-GelMA, we observed a 15% increase in the

O.D. value from 1 to 3 days, a 5% increase from 3 to 7 days, and a 3% increase from 7 to 10 days. These results indicate that the hDPSCs maintained their viability and proliferation capability in the bioprinted dental constructs in both the GelMA and BMP-GelMA constructs. Furthermore, there was no significant difference in hDPSC viability or proliferation between the GelMA and BMP-GelMA constructs, indicating that the BMP-mimetic peptide did not have an obvious influence on cell viability and proliferation.

3.4. Histological and immunofluorescent analyses of the bioprinted dental constructs

To investigate the effect of BMP-mimetic peptide on hDPSC differentiation, the bioprinted hDPSCs-laden GelMA and BMP-GelMA constructs were cultured and analyzed at 2 or 4 weeks in either NGM, OM or OM-D. Cell morphology and ECM production were examined by H&E staining (Figure 4A). According to the H&E staining results, cells were evenly distributed at both 2 and 4 weeks, which implies the cells maintained their homogeneous distribution in the bioink during the culture.

In the Alizarin Red S stained sections (Figure 4B), no calcium deposition in the constructs was observed at 2 weeks in any of the cultured construct groups. By 4 weeks, weak calcium deposition was observed in all of the constructs except for those cultured in GelMA without BMP peptide in NGM. For the 4-week constructs, calcified AR stained areas were 34% for GelMA without BMP peptide in OM, 12% for BMP-GelMA in NGM, 49% for BMP-GelMA in OM-D, and 55% for BMP-GelMA in OM (Figure 4C). The BMP-mimetic peptide conjugation groups exhibited higher AR stained areas as compared to their non-BMP counterparts, and even induced small amounts of calcified tissue matrix formation in the NGM group. These results indicated that the BMP-mimetic peptide could promote hDPSC differentiation in *in vitro* cell culture.

Immunofluorescent staining of sectioned GelMA and BMP-GelMA constructs was performed to investigate DSPP and OCN expression in the 3D bioprinted dental constructs (Figure 5A). At 2 weeks, only slight positive staining for DSPP and OCN was observed. The levels of expression remained unchanged at 4 weeks for the GelMA without BMP peptide in NGM group, while in contrast, the GelMA with OM, and the BMP-GelMA constructs cultured using all medium conditions, showed strong DSPP (red) and OCN (green) expression, indicating hDPSC differentiation. DSPP and OCN expressions were quantified in the 4-week cultured construct groups by measuring red and green stained areas as a percentage of the total tissue area (Figure 5C,D). Overall, BMP-GelMA groups showed higher DSPP and OCN expression as compared to GelMA alone groups under similar NGM conditions. DSPP and OCN expression patterns were similar between GelMA alone construct cultured in OM, and BMP-GelMA constructs cultured in NGM, suggesting that BMP conjugation could compensate for the lack of osteogenic factors in the tissue culture medium. Within the BMP-GelMA group, constructs cultured in OM-D showed increased DSPP and OCN expression levels as compared to BMP-GelMA constructs cultured in NGM. Expression levels increased even further in OM cultured BMP-GelMA constructs, indicating that conjugated BMP has a synergistic effect when used along with osteogenic differentiation culture medium. These results agree well with the observed Alizarin Red

staining results, which together, suggest that BMP mimicking peptide can promote osteogenic gene expression in *in vitro* cultured 3D bioprinted dental constructs.

3.5. qRT-PCR analysis

Quantitative RT-PCR analyses were conducted on 3D bioprinted dental constructs (Figure 6). Constructs were assessed for expression of the odontogenic marker DSPP and osteogenic markers collagen type 1, Runx2, BGLAP (OCN), as compared to the housekeeping gene GAPDH. Collagen type 1 (COL1A1) and Runx2 are early markers for osteogenic differentiation, and are expressed prior to mineralization. After 2 weeks, we observed a significant increase in the expression of Runx2 in the BMP-GelMA NGM group compared with GelMA NGM group. Little to no change in gene expression was observed at 2 weeks for COL1A1, DSPP, and BGLAP. After 4 weeks, the expression of COL1A1 and BGLAP mRNA increased in all groups. The expression level of COL1A1 mRNA was significantly higher in the BMP-GelMA groups for all medium conditions, as compared to the GelMA OM group. For BLGAP, the BMP OM and BMP OM-D groups exhibited 1.5 to 2 times fold higher expression levels as compared to the GelMA OM group. In particular, the BMP-GelMA NGM group exhibited 7-fold higher DSPP and 3-fold higher BGLAP expression levels as compared to GelMA NGM constructs. The expression level of DSPP was slightly higher in the BMP-GelMA groups for all medium conditions; however, there were no significant differences.

4. Discussion

In cases of facial trauma, no two defects are similar in size or shape. In addition, achieving aesthetic symmetry of repaired craniofacial defects is especially important. As such, 3D bioprinting is particularly advantageous for manufacturing precise 3D constructs with regional specificity (28, 42, 43), capabilities that are essential for targeted regeneration of complex, multi-tissue craniofacial defects such as the jaw bone and tooth interface. For this purpose, we aimed to develop a BMP-mimetic peptide-conjugated odontogenic-specific bioink for 3D bioprinting of hDPSCs, to fabricate dental constructs. We hypothesized that BMP-mimetic peptide could enhance the differentiation of hDPSCs within the bioprinted dental constructs.

In this study, we used the thiolated BMP peptide that could simply conjugate with the double bonds in the GelMA hydrogel during the UV light crosslinking, thereby providing long-term stability and effectiveness of the BMP peptide in the 3D bioprinted constructs. The stability experiment of FITC-labeled BMP-SH showed stable conjugation to the GelMA up to 3 weeks incubation, with over 40% of BMP-SH remaining in the bioprinted dental constructs at 4 weeks. Moreover, BMP-conjugation did not significantly affect the bioink's degradation profile, swelling ratio, or mechanical properties before or after UV crosslinking. Cell viability and cell proliferation were high in constructs with and without BMP-conjugation. Therefore, by simple mixing with the GelMA, we found that BMP-SH could be incorporated into the GelMA bioink without impacting the bioink's basic properties. This is a significant benefit as it makes the incorporation of BMP-SH into bioinks an easy and straightforward process. Additionally, these results also suggest that any differences found

between GelMA and BMP-GelMA groups were caused directly by BMP-SH activity, rather than indirectly through more broad differences in the bioink's properties.

We tested the effect of BMP-conjugated GelMA constructs on the differentiation of hDPSCs using histological, immunofluorescence, and qRT-PCR analyses. H&E staining confirmed the homogenous distribution of hDPSCs and the elaboration of mineralized tissue matrix production in all groups. Alizarin Red staining showed higher calcium deposition in the BMP-GelMA groups as compared OM conditions. A small increase in calcium deposition was observed in BMP-GelMA constructs were cultured in the NGM, indicating that BMP-conjugation was at least partially able to drive odontogenic differentiation of hDPSCs independently of differentiation factors in the OM conditions. A small increase in calcium deposition was observed in BMP-GelMA constructs were cultured in the NGM, indicating that BMP-conjugation was at least partially able to drive odontogenic differentiation of hDPSCs independently of differentiation factors in the media. A modest increase was also seen in the bioprinted constructs cultured in the OM medium, indicating that the inclusion of BMP-conjugation could have a synergistic effect when combined with the OM medium.

Similar results were obtained for the immunofluorescence analyses of DSPP and OCN expression in the bioprinted dental constructs. Expression of both DSPP and OCN were higher in the BMP-GelMA groups than in the GelMA alone groups. When quantified, these results tracked very closely with those obtained using Alizarin Red staining. These results further support the conclusion that the addition of BMP-conjugation to GelMA bioinks can increase the odontogenic/osteogenic behavior of hDPSCs both independently of, and synergistically with, the differentiation media. In particular, the DSPP immunostaining suggests the BMP-conjugation may have potential in dental applications in addition to those in the bone.

The results of qRT-PCR confirmed that the BMP-GelMA groups expressed more odontogenic and osteogenic differentiation mRNAs than the GelMA groups. When comparing groups with similar media conditions, hDPSCs in BMP-GelMA constructs showed similar Runx2 expression, slightly more COL1A1 expression, and significantly more DSPP and OCN expression than their GelMA only counterparts. Comparing within bioink groups and across different media conditions, expression of all four markers was increased in the OM condition relative to NGM condition, which is consistent with the existing body of literature.

We investigated whether the BMP peptide could induce osteogenic differentiation in the medium lacking dexamethasone. Because dexamethasone among the osteogenic supplements has been known for its necessity in promoting the osteogenic differentiation of stem cells cultured *in vitro* (44, 45). However, it has been known that the proliferation ability of stem cells in the dexamethasone decreases during the long-term osteogenic culture (46, 47). Since a limited number of stem cells could be obtained from the donor, it would be beneficial to culture stem cells *in vitro* in the absence of dexamethasone for osteogenic differentiation (44). In this study, we demonstrated that the OM-D group (absence of dexamethasone) in the BMP-GelMA showed significantly higher osteogenic capability as compared to the OM group in the GelMA constructs. Moreover, there was no significant

difference between the OM-D and OM conditions in the BMP-GelMA constructs, excluding DSPP expression.

The development of tissue-specific bioinks would be highly beneficial for regenerating 3D bioprinted multi-dimensional constructs similar to native tissues and organs (48). The results of this study indicate that this BMP-mimetic peptide, when tethered to GelMA via simple thiol introduction and UV crosslinking, can provide an odontogenic microenvironment within the bioprinted constructs. Future work could look to improve upon the long-term stability of the BMP-mimetic peptide in culture, and in *in vivo* implanted constructs, as well as its odontogenic capabilities. Efforts to continually improve the local odontogenic microenvironment within the bioprinted dental constructs using complementary strategies will also likely be necessary to reach the clinical application. Further, *in vivo* considerations such as the host immune response, GelMA degradation, and construct vascularization will need to be taken into account (49). Finally, additional studies will need to be conducted to investigate whether this strategy can be used to induce regional differences in cell behavior within constructs.

5. Conclusions

Here we describe the development of a novel BMP-mimetic peptide-tethering bioink for 3D bioprinted bioengineered dental tissue constructs. This bioink formulation provided proper printability and dental-specific microenvironment to support hDPSC differentiation. The results from this study showed that the BMP-GelMA bioink formulation supported high hDPSC viability and proliferation, and accelerated their odontogenic differentiation in 3D bioprinted constructs. Together, these results demonstrate that 3D bioprinting strategies, combined with a novel BMP-peptide-tethered bioink, have great potential to create bioengineered dental tissue constructs for use in future applications in regenerative medicine and dentistry.

Supplementary Material

Refer to Web version on PubMed Central for supplementary material.

Acknowledgments

This study was supported by NIH/NIBIB 1P41EB023833 and NIH/NIDCR/NIBIB R01DE026731.

References

1. Mitchener TA, Chan R, Simecek JW. Oral-Maxillofacial Injury Surveillance of U.S. Military Personnel in Iraq and Afghanistan, 2001 to 2014. Mil Med. 2017;182(3):e1767–e73. [PubMed: 28290957]
2. Moses H, Powers D, Keeler J, Erdmann D, Marcus J, Puscas L, et al. Opportunity Cost of Surgical Management of Craniomaxillofacial Trauma. Craniomaxillofac Trauma Reconstr. 2016;9(1):76–81. [PubMed: 26889352]
3. Krisam J, Ott L, Schmitz S, Klotz AL, Seyidaliyeva A, Rammelsberg P, et al. Factors affecting the early failure of implants placed in a dental practice with a specialization in implantology - a retrospective study. BMC Oral Health. 2019;19(1):208. [PubMed: 31488110]

4. Young CS, Terada S, Vacanti JP, Honda M, Bartlett JD, Yelick PC. Tissue engineering of complex tooth structures on biodegradable polymer scaffolds. J Dent Res. 2002;81(10):695–700. [PubMed: 12351668]
5. Abukawa H, Zhang W, Young CS, Asrican R, Vacanti JP, Kaban LB, et al. Reconstructing mandibular defects using autologous tissue-engineered tooth and bone constructs. J Oral Maxillofac Surg. 2009;67(2):335–47. [PubMed: 19138608]
6. Smith EE, Angstadt S, Monteiro N, Zhang W, Khademhosseini A, Yelick PC. Bioengineered Tooth Buds Exhibit Features of Natural Tooth Buds. J Dent Res. 2018;97(10):1144–51. [PubMed: 29879370]
7. Zhang W, Vazquez B, Yelick PC. Bioengineered post-natal recombinant tooth bud models. J Tissue Eng Regen Med. 2017;11(3):658–68. [PubMed: 25424341]
8. Kang H-W, Lee SJ, Ko IK, Kengla C, Yoo JJ, Atala A. A 3D bioprinting system to produce human-scale tissue constructs with structural integrity. Nature Biotechnology. 2016;34:312.
9. Moroni L, Burdick JA, Highley C, Lee SJ, Morimoto Y, Takeuchi S, et al. Biofabrication strategies for 3D in vitro models and regenerative medicine. Nat Rev Mater. 2018;3(5):21–37. [PubMed: 31223488]
10. Murphy SV, Atala A. 3D bioprinting of tissues and organs. Nat Biotechnol. 2014;32(8):773–85. [PubMed: 25093879]
11. Seol Y-J, Kang H-W, Lee SJ, Atala A, Yoo JJ. Bioprinting technology and its applications. European Journal of Cardio-Thoracic Surgery. 2014;46(3):342–8. [PubMed: 25061217]
12. Hölzl K, Lin S, Tytgat L, Van Vlierberghe S, Gu L, Ovsianikov A. Bioink properties before, during and after 3D bioprinting. Biofabrication. 2016;8(3):032002. [PubMed: 27658612]
13. Du M, Chen B, Meng Q, Liu S, Zheng X, Zhang C, et al. 3D bioprinting of BMSC-laden methacrylamide gelatin scaffolds with CBD-BMP2-collagen microfibers. Biofabrication. 2015;7(4):044104. [PubMed: 26684899]
14. Lee VK, Kim DY, Ngo H, Lee Y, Seo L, Yoo S-S, et al. Creating perfused functional vascular channels using 3D bio-printing technology. Biomaterials. 2014;35(28):8092–102. [PubMed: 24965886]
15. Huang J, Fu H, Wang Z, Meng Q, Liu S, Wang H, et al. BMSCs-laden gelatin/sodium alginate/carboxymethyl chitosan hydrogel for 3D bioprinting. Rsc Advances. 2016;6(110):108423–30.
16. Wang Z, Lee SJ, Cheng HJ, Yoo JJ, Atala A. 3D bioprinted functional and contractile cardiac tissue constructs. Acta Biomater. 2018;70:48–56. [PubMed: 29452273]
17. Gao T, Gillispie GJ, Copus JS, Pr AK, Seol YJ, Atala A, et al. Optimization of gelatin-alginate composite bioink printability using rheological parameters: a systematic approach. Biofabrication. 2018;10(3):034106. [PubMed: 29923501]
18. Gao G, Schilling AF, Hubbell K, Yonezawa T, Truong D, Hong Y, et al. Improved properties of bone and cartilage tissue from 3D inkjet-bioprinted human mesenchymal stem cells by simultaneous deposition and photocrosslinking in PEG-GelMA. Biotechnology letters. 2015;37(11):2349–55. [PubMed: 26198849]
19. Yue K, Trujillo-de Santiago G, Alvarez MM, Tamayol A, Annabi N, Khademhosseini A. Synthesis, properties, and biomedical applications of gelatin methacryloyl (GelMA) hydrogels. Biomaterials. 2015;73:254–71. [PubMed: 26414409]
20. Bertassoni LE, Cardoso JC, Manoharan V, Cristino AL, Bhise NS, Araujo WA, et al. Direct-write bioprinting of cell-laden methacrylated gelatin hydrogels. Biofabrication. 2014;6(2):024105. [PubMed: 24695367]
21. Yin J, Yan M, Wang Y, Fu J, Suo H. 3D bioprinting of low-concentration cell-laden gelatin methacrylate (GelMA) bioinks with a two-step cross-linking strategy. ACS applied materials & interfaces. 2018;10(8):6849–57. [PubMed: 29405059]
22. McBeth C, Lauer J, Ottersbach M, Campbell J, Sharon A, Sauer-Budge AF. 3D bioprinting of GelMA scaffolds triggers mineral deposition by primary human osteoblasts. Biofabrication. 2017;9(1):015009. [PubMed: 28071596]
23. Pati F, Jang J, Ha D-H, Kim SW, Rhie J-W, Shim J-H, et al. Printing three-dimensional tissue analogues with decellularized extracellular matrix bioink. Nature communications. 2014;5:3935.

24. Skardal A, Devarasetty M, Kang H-W, Mead I, Bishop C, Shupe T, et al. A hydrogel bioink toolkit for mimicking native tissue biochemical and mechanical properties in bioprinted tissue constructs. Acta biomaterialia. 2015;25:24–34. [PubMed: 26210285]
25. Gao G, Lee JH, Jang J, Lee DH, Kong JS, Kim BS, et al. Tissue engineered bio-blood-vessels constructed using a tissue-specific bioink and 3D coaxial cell printing technique: a novel therapy for ischemic disease. Advanced Functional Materials. 2017;27(33):1700798.
26. Ma Y, Ji Y, Zhong T, Wan W, Yang Q, Li A, et al. Bioprinting-based PDLSC-ECM screening for in vivo repair of alveolar bone defect using cell-laden, injectable and photocrosslinkable hydrogels. ACS Biomaterials Science & Engineering. 2017;3(12):3534–45.
27. Ma Y, Ji Y, Huang G, Ling K, Zhang X, Xu F. Bioprinting 3D cell-laden hydrogel microarray for screening human periodontal ligament stem cell response to extracellular matrix. Biofabrication. 2015;7(4):044105. [PubMed: 26696269]
28. Ren K, He C, Xiao C, Li G, Chen X. Injectable glycopolypeptide hydrogels as biomimetic scaffolds for cartilage tissue engineering. Biomaterials. 2015;51:238–49. [PubMed: 25771014]
29. Balakrishnan B, Joshi N, Jayakrishnan A, Banerjee R. Self-crosslinked oxidized alginate/gelatin hydrogel as injectable, adhesive biomimetic scaffolds for cartilage regeneration. Acta biomaterialia. 2014;10(8):3650–63. [PubMed: 24811827]
30. Wu S, Liu X, Yeung KW, Liu C, Yang X. Biomimetic porous scaffolds for bone tissue engineering. Materials Science and Engineering: R: Reports. 2014;80:1–36.
31. Grasman JM, Zayas MJ, Page RL, Pins GD. Biomimetic scaffolds for regeneration of volumetric muscle loss in skeletal muscle injuries. Acta biomaterialia. 2015;25:2–15. [PubMed: 26219862]
32. Lo KW, Ulery BD, Ashe KM, Laurencin CT. Studies of bone morphogenetic protein-based surgical repair. Adv Drug Deliv Rev. 2012;64(12):1277–91. [PubMed: 22512928]
33. Holloway JL, Ma H, Rai R, Burdick JA. Modulating hydrogel crosslink density and degradation to control bone morphogenetic protein delivery and in vivo bone formation. Journal of Controlled Release. 2014;191:63–70. [PubMed: 24905414]
34. El Bialy I, Jiskoot W, Nejadnik MR. Formulation, delivery and stability of bone morphogenetic proteins for effective bone regeneration. Pharmaceutical research. 2017;34(6):1152–70. [PubMed: 28342056]
35. He X, Ma J, Jabbari E. Effect of grafting RGD and BMP-2 protein-derived peptides to a hydrogel substrate on osteogenic differentiation of marrow stromal cells. Langmuir. 2008;24(21):12508–16. [PubMed: 18837524]
36. Madl CM, Mehta M, Duda GN, Heilshorn SC, Mooney DJ. Presentation of BMP-2 mimicking peptides in 3D hydrogels directs cell fate commitment in osteoblasts and mesenchymal stem cells. Biomacromolecules. 2014;15(2):445–55. [PubMed: 24400664]
37. Mercado AE, Yang X, He X, Jabbari E. Effect of grafting BMP2-derived peptide to nanoparticles on osteogenic and vasculogenic expression of stromal cells. J Tissue Eng Regen Med. 2014;8(1):15–28. [PubMed: 22764116]
38. Zhou X, Feng W, Qiu K, Chen L, Wang W, Nie W, et al. BMP-2 Derived Peptide and Dexamethasone Incorporated Mesoporous Silica Nanoparticles for Enhanced Osteogenic Differentiation of Bone Mesenchymal Stem Cells. ACS Appl Mater Interfaces. 2015;7(29):15777–89. [PubMed: 26133753]
39. Brounts SH, Lee JS, Weinberg S, Lan Levengood SK, Smith EL, Murphy WL. High affinity binding of an engineered, modular peptide to bone tissue. Mol Pharm. 2013;10(5):2086–90. [PubMed: 23506396]
40. Zhang X, Guo WG, Cui H, Liu HY, Zhang Y, Muller WE, et al. In vitro and in vivo enhancement of osteogenic capacity in a synthetic BMP-2 derived peptide-coated mineralized collagen composite. J Tissue Eng Regen Med. 2016;10(2):99–107. [PubMed: 23364810]
41. He X, Yang X, Jabbari E. Combined effect of osteopontin and BMP-2 derived peptides grafted to an adhesive hydrogel on osteogenic and vasculogenic differentiation of marrow stromal cells. Langmuir. 2012;28(12):5387–97. [PubMed: 22372823]
42. Tarafder S, Koch A, Jun Y, Chou C, Awadallah MR, Lee CH. Micro-precise spatiotemporal delivery system embedded in 3D printing for complex tissue regeneration. Biofabrication. 2016;8(2):025003. [PubMed: 27108484]

43. Li X, Ding J, Wang J, Zhuang X, Chen X. Biomimetic biphasic scaffolds for osteochondral defect repair. Regenerative biomaterials. 2015;2(3):221–8. [PubMed: 26816644]

44. Holtorf HL, Jansen JA, Mikos AG. Flow perfusion culture induces the osteoblastic differentiation of marrow stroma cell-scaffold constructs in the absence of dexamethasone. J Biomed Mater Res A. 2005;72(3):326–34. [PubMed: 15657936]

45. Thibault RA, Scott Baggett L, Mikos AG, Kasper FK. Osteogenic differentiation of mesenchymal stem cells on pregenerated extracellular matrix scaffolds in the absence of osteogenic cell culture supplements. Tissue Eng Part A. 2010;16(2):431–40. [PubMed: 19863274]

46. Atmani H, Audrain C, Mercier L, Chappard D, Basle MF. Phenotypic effects of continuous or discontinuous treatment with dexamethasone and/or calcitriol on osteoblasts differentiated from rat bone marrow stromal cells. J Cell Biochem. 2002;85(3):640–50. [PubMed: 11968004]

47. Porter RM, Huckle WR, Goldstein AS. Effect of dexamethasone withdrawal on osteoblastic differentiation of bone marrow stromal cells. J Cell Biochem. 2003;90(1):13–22. [PubMed: 12938152]

48. Wang B, Yao M, Lv L, Ling Z, Li L. The human microbiota in health and disease. Engineering. 2017;3(1):71–82.

49. Daly AC, Pitacco P, Nulty J, Cunniffe GM, Kelly DJ. 3D printed microchannel networks to direct vascularisation during endochondral bone repair. Biomaterials. 2018;162:34–46. [PubMed: 29432987]

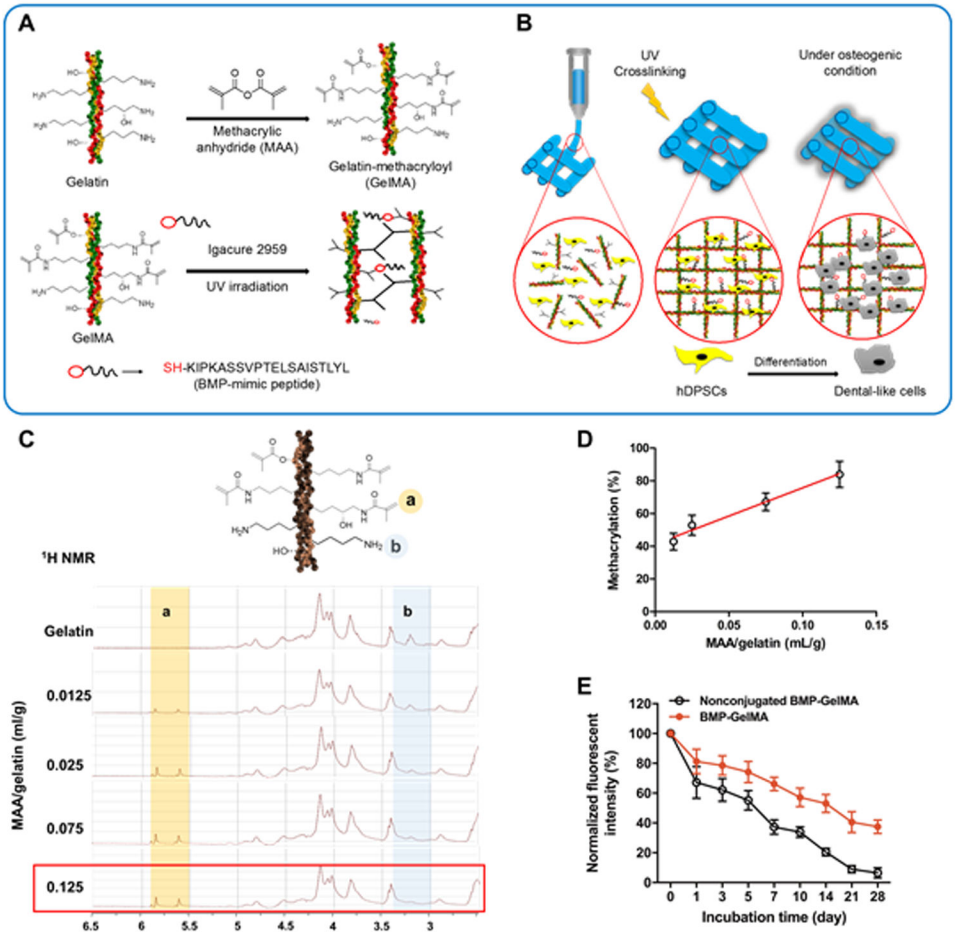

Figure 1. Gelatin methacrylation process and conjugation of BMP-mimetic peptide to GelMA.

(A) Gelatin is methacrylated using methacrylic anhydride (MAA) to create GelMA. GelMA is then crosslinked and a synthetic BMP-peptide containing a thiol group (-SH) is bound to the GelMA in the presence of photoinitiator and UV irradiation. (B) Conceptual design of the bioprinting process used in this study. Bioinks containing GelMA, hDPSCs, and BMP-SH were extrusion bioprinted and then UV crosslinked. During *in vitro* cell culture, hDPSCs differentiate into odontogenic-like cells. (C) ^{1}H NMR analysis of GelMA synthesis with different amounts of MAA/gelatin (mL/g). (D) Percent (%) methacrylation of GelMA is dependent on MAA amount (n=3 per group). (E) Normalized fluorescent intensity of FITC-BMP-conjugated GelMA constructs (n=3 per group). All data represented as mean ± SD.

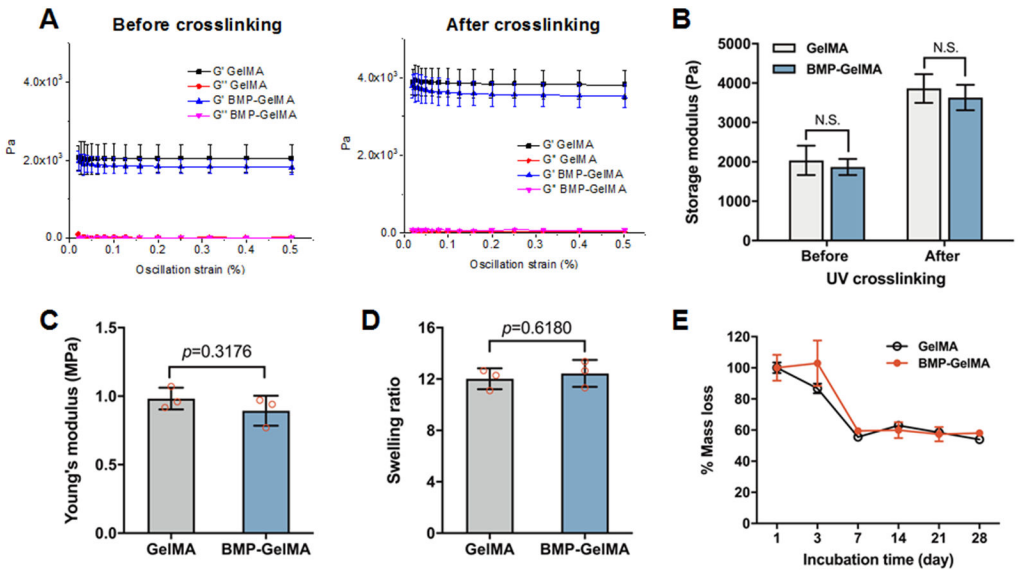

Figure 2. Mechanical Properties of GelMA and BMP-GelMA constructs.

(A) Storage modulus (G') and loss modulus (G") as measured via strain sweep. GelMA was tested both with and without BMP-conjugation and before and after crosslinking. (B) The storage modulus of GelMA with and without BMP-conjugation, before and after crosslinking (n=15 per group). (C) Young's modulus of crosslinked GelMA with and without BMP-conjugation measured via compression test (n=3 per group). (D) The swelling ratio of GelMA bioink with and without conjugated BMP (n=3 per group). (E) Percent mass lost over time of GelMA bioink with and without BMP-conjugation (n=3 per group). All data represented as mean ± SD. The p-values by a two-sided Student t-test are indicated. N.S. indicates no significance.

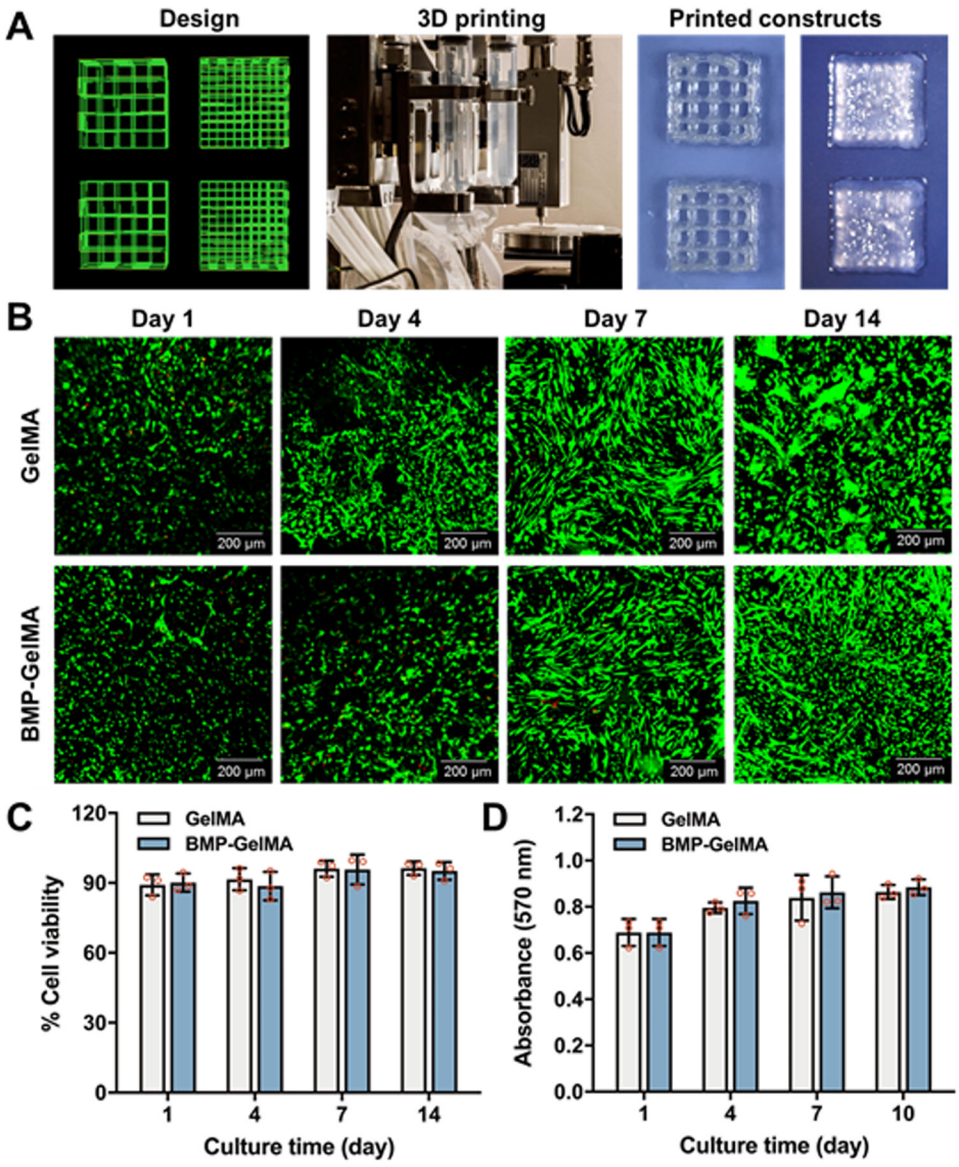

Figure 3. Human DPSC viability and proliferation in the bioprinted constructs.

(A) Schematic of printing code, photograph of bioprinting set-up, and printed lattice and solid cuboidal constructs. (B) Live/dead staining of hDPSCs in the bioprinted constructs at 1, 4, 7, and 14 days after printing (n=3 per group). (C) Quantification of percent cell viability. (D) Cell proliferation of hDPSCs within bioprinted constructs (n=3 per group). All data represented as mean ± SD.

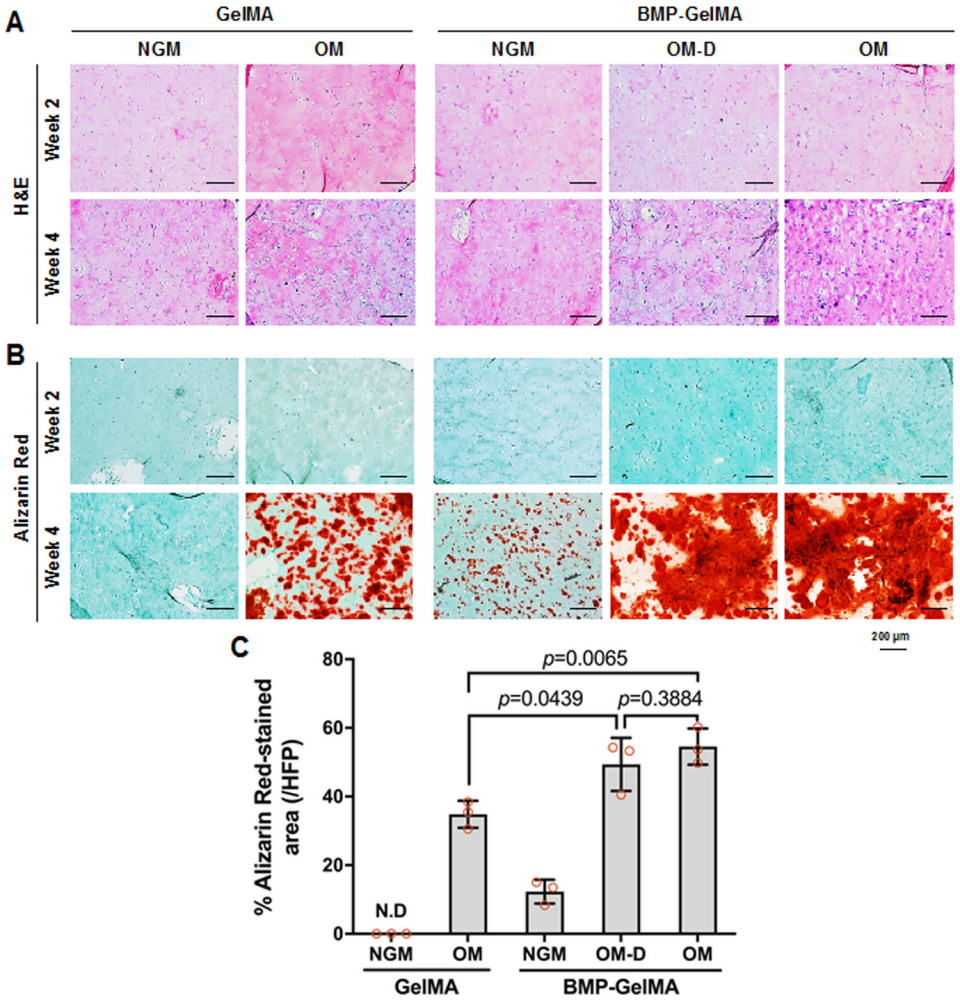

Figure 4. Osteogenic differentiation of hDPSCs in 3D dental constructs.

(A) H&E and (B) Alizarin Red staining of 3D bioprinted dental constructs after 2 and 4 weeks under different media *in vitro* culture and bioink conditions. (C) Quantification of Alizarin Red staining assay (n=3 per group). All data represented as mean ± SD. The p-values by two-way ANOVA followed by Turkey's test are indicated. NGM: normal growth medium, OM: osteogenic medium, OM-D: OM without dexamethasone.

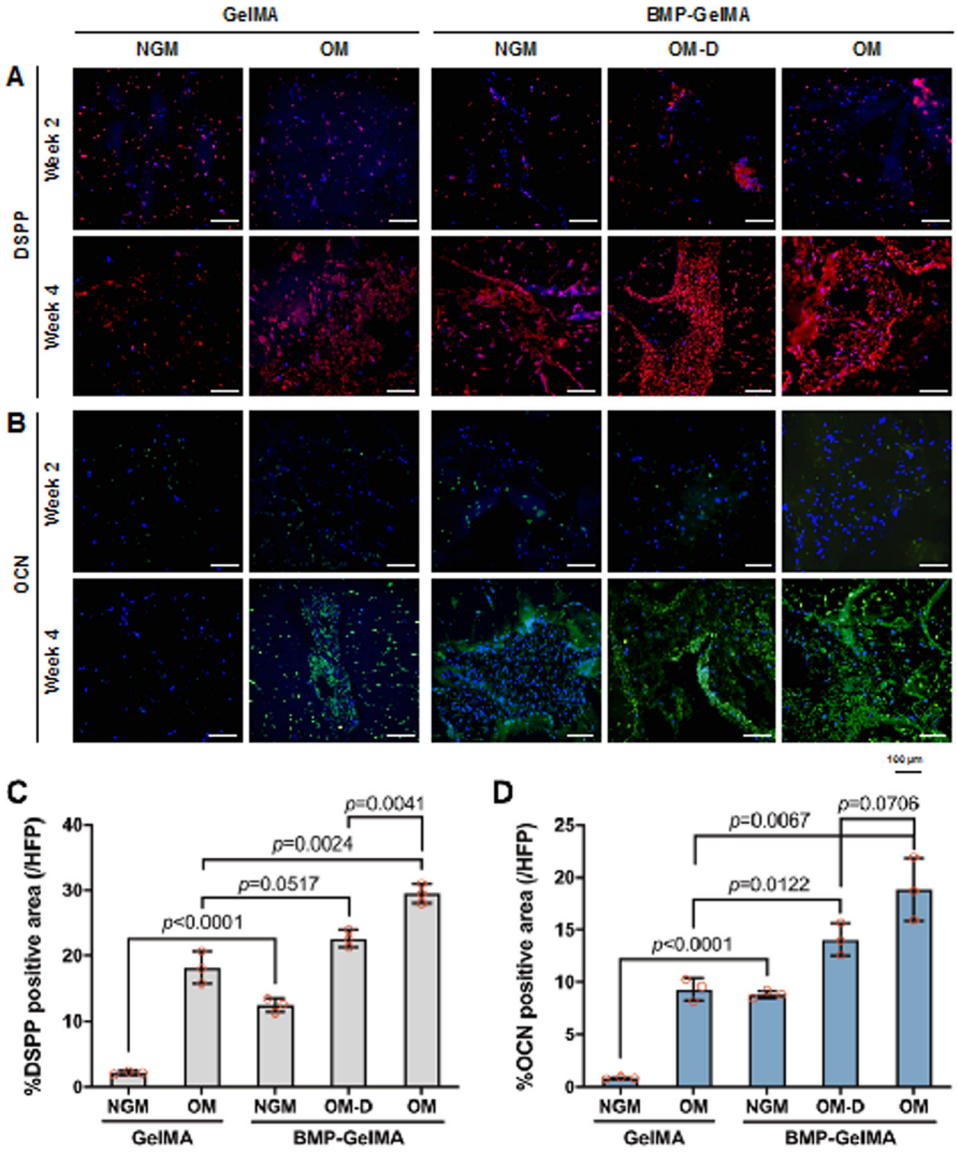

Figure 5. Osteogenic differentiation marker expression of in vitro cultured 3D bioprinted dental constructs.

Immunofluorescent staining of (A) DSPP and (B) OCN expression in bioprinted constructs after 2 and 4 weeks under different media and bioink conditions. Quantification of (C) DSPP and (D) OCN expression (n=3 per group). All data represented as mean ± SD. The p-values by two-way ANOVA followed by Turkey's test are indicated. NGM: normal growth medium, OM: osteogenic medium, OM-D: OM without dexamethasone.

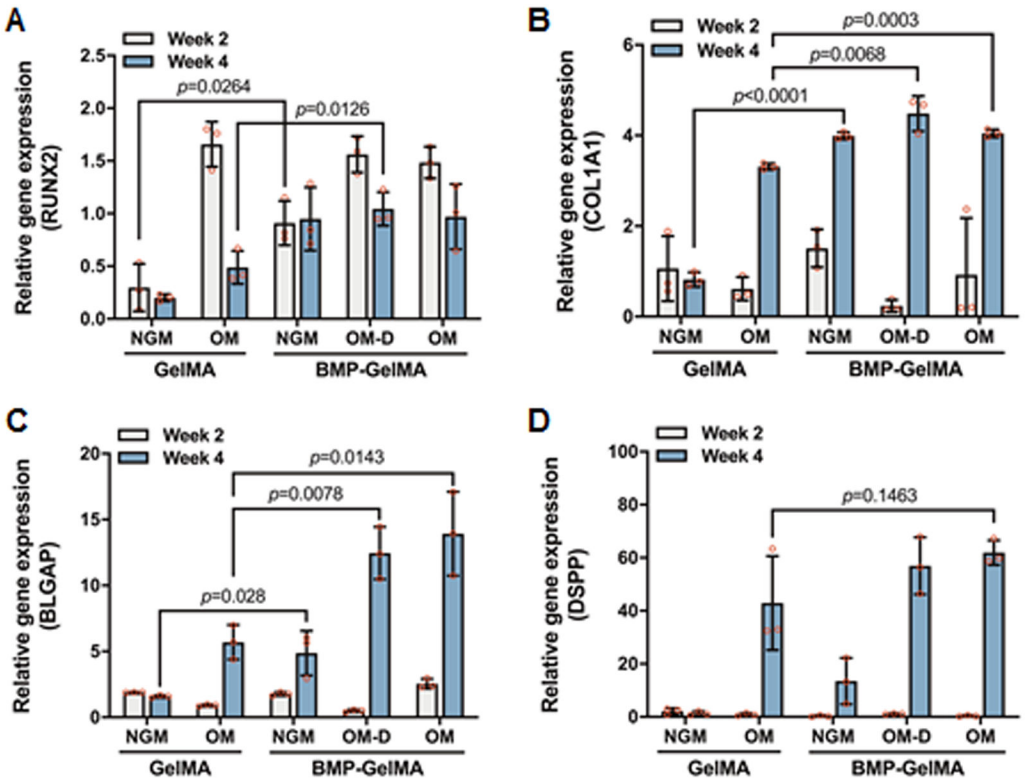

Figure 6. qRT-PCR analyses of in vitro cultured 3D printed dental constructs.

Gene expression of DPSCs in bioprinted constructs with and without BMP-conjugation of (A) RUNX2, (B) COL1A1, (C) BGLAP, and (D) DSPP at 2 and 4 weeks under various media conditions (n=3 per group). All data represented as mean ± SD. The p-values by two-way ANOVA followed by Turkey's test are indicated. NGM: normal growth medium, OM: osteogenic medium, OM-D: OM without dexamethasone.

Table 1.

Human primer sequences used for RT-PCR of bioprinted constructs

Genes	Primer Sequence	
	Forward 5'-3'	Reverse 5'-3'
GAPDH	GGAGCGAGATCCCTCCAAAAT	GGCTGTTGTCATACTTCTCATGG
RUNX2	TGGTTACTGTCATGGCGGGTA	TCTCAGATCGTTGAACCTTGCTA
BGLAP (OCN)	CGCTACCTGTATCAATGGCTGG	CTCCTGAAAGCCGATGTGGTCA
DSPP	TTTGGGCAGTAGCATGGGC	CCATCTTGGGTATTCTCTTGCCT
COL1A1	GAGGGCCAAGACGAAGACATC	CAGATCACGTCATCGCACAAC